

Explaining Optomechanical Libration Spectra: A Stochastic Simulation Approach

Ankush Gogoi,¹ Vikram Pakrashi,¹ and Joanna A. Zielińska^{2,*}

¹*UCD Centre for Mechanics, School of Mechanical and Materials Engineering, University College Dublin, Dublin, Ireland*

²*School of Engineering and Sciences, Tecnológico de Monterrey, Monterrey, N.L., Mexico*

In this work, we present a practical and computationally effective Ito-Taylor expansion based stochastic simulation framework for modeling rotational optomechanics experiments. By developing a model using this framework, we could capture the nonlinear orientation dynamics of an optically levitated, nearly cylindrically symmetric nanodumbbell. It successfully reproduces and explains shoulder-like features observed in the power spectral density of libration, which we show arising from the interplay between confined libration and thermally driven rotation around the particle's symmetry axis.

I. INTRODUCTION

The study of the dynamics of nano and microscale objects levitated in vacuum has rapidly developed into a versatile platform for sensing weak forces and torques, testing macroscopic quantum phenomena, and searching for physics beyond the standard model [1, 2]. While control over the center-of-mass (COM) motion of particles around 100 nm in size is steadily advancing toward the quantum regime [3], increasing attention is being directed toward the rotational degrees of freedom of levitated anisotropic nanoparticles. Recent progress in this area includes quantum ground-state cooling of torsional oscillations (libration) [4], coupling to internal spin degrees of freedom [5], record-setting torque sensitivities [6], and interactions with the transverse orbital angular momentum of light [7], among other notable achievements.

In certain cases, the alignment dynamics of an optically levitated nanoparticle can closely resemble center-of-mass motion, effectively acting like harmonic oscillators. This occurs for non-cylindrically symmetric particles (typically multi-particle clusters comparable in size to the optical trap), where all three librational degrees of freedom are tightly confined, resulting in clean Lorentzian power spectral densities with minimal cross-coupling [8–10]. In contrast, smaller particles such as dumbbells, composed of two nanospheres, exhibit only two confined libration modes under linearly polarized optical tweezers, while the third mode remains effectively free. This results in spectral features that differ from those expected for fully harmonically confined systems.

However, even in the simplest case of nanodumbbell libration in linearly polarized optical tweezers, a variety of libration power spectral densities (PSDs) have been reported in the literature. These include single Lorentzian peaks [11], Lorentzian peaks with shoulder-like features [12–15], as well as irregular, split spectral structures [6, 16, 17]. Clearly, the shape of these spectra is highly sensitive to precise experimental conditions such as deviations from perfect cylindrical symmetry of

the particle, and the exact intensity and polarization profile of the optical field gives rise to both conservative and non-conservative torques.

The inherent nonlinearity and stochastic nature of the system make theoretical modeling of rotational degrees of freedom in levitated optomechanics particularly challenging. Accurate simulations must account for the full three-dimensional rotational dynamics of the particle, incorporating stochastic thermal torques, an often complex optical potential landscape, and nonlinear terms describing the coupling between the various degrees of freedom.

A fundamental framework for describing the dynamics of nonlinear systems subjected to random external forces is provided by stochastic differential equations (SDEs) [18, 19]. Numerical integration schemes based on Ito-Taylor expansion have proven effective for solving nonlinear SDEs across a wide range of applications [20–22].

In this work, we introduce a computationally efficient stochastic simulation framework based on Ito-Taylor expansion that captures the nonlinear, three-dimensional orientation dynamics of levitated nearly cylindrically symmetric particles. By modeling both deterministic and thermal torques in realistic optical fields, we are able to reproduce and explain shoulder-like features observed in the libration PSD of nanodumbbell-shaped rotors. We show that these spectral signatures originate from the interplay between confined and thermally fluctuating rotation around the particle's symmetry axis.

Our stochastic simulation approach has the potential to become essential for supporting a wide range of applications, including high-precision torque sensing [6], the development of levitated gyroscopes [23], and the study of macroscopic quantum rotational phenomena [24].

This paper is structured as follows. In Sec. II, we describe the orientational dynamics of a levitated nanoparticle. We discuss the equations of motion and the approximations we employ. Next, in Section III, we present the stochastic simulation framework based on stochastic Ito-Taylor expansion. Throughout Section IV, we compare the simulation results with experimental data, and Section V concludes the paper.

* jzielinska@tec.mx

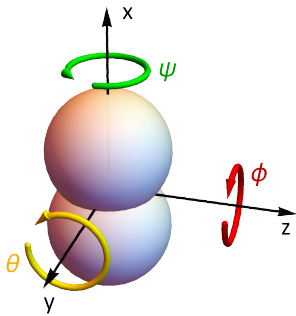


Figure 1. Rotational degrees of freedom of a nanodumbbell with its long axis aligned along the laboratory x -axis. In a typical levitated optomechanics setup with the optical tweezers beam propagating along the z -axis, the time-dependent behavior of the angle ϕ , representing the orientation of the long axis in the xy -plane, is measured.

II. DESCRIPTION OF THE DYNAMICS

We first outline the physical characteristics of the nanodumbbell and introduce the formalism used to describe its rotational degrees of freedom. We then describe the orientation-dependent optical potential resulting from the particle's anisotropic geometry. Finally, we present the stochastic equations of motion governing the rotational dynamics and discuss the role of thermally fluctuating torques that drive the system.

This work focuses on a nearly cylindrically symmetric nanodumbbell made of two dielectric nanospheres. We denote $\boldsymbol{\alpha} = \text{diag}(\alpha_1, \alpha_2, \alpha_3)$ and $\mathbf{I} = \text{diag}(I_1, I_2, I_3)$ as the static electric polarizability and inertia tensors of the object in the intrinsic body frame, respectively, assuming $\alpha_1 \approx \alpha_2 \leq \alpha_3$ and $I_1 \approx I_2 \geq I_3$. We refer to the principal axis with the largest polarizability and the smallest moment of inertia as the “long axis” of the object. In order to describe the orientation of the body reference frame with respect to the laboratory frame (x, y, z), we use the intrinsic x -convention of Euler angles denoted as ϕ , θ and ψ (see [25] and §35 in [26]), as illustrated in Fig. 1. The Euler angles ϕ and θ define the orientation of the rotor's long axis, while ψ describes the rotation around the long axis, indicating the orientation of the intermediate axis, associated with the intermediate moment of inertia. In a typical levitated optomechanics experiment, with optical tweezers beam propagating along z , the only Euler angle accessible to measurement is ϕ , corresponding to the orientation of the long axis in the xy -plane [27].

The nanodumbbell is trapped by an optical tweezers beam propagating along the z -axis and linearly polarized along the x -axis. We assume that the particle's centre of mass (COM) remains fixed at the center of the optical trap. The anisotropic electric polarizability of the nanodumbbell gives rise to libration dynamics. The rotor's long axis undergoes two-dimensional libration os-

cillations around its equilibrium orientation, aligned with the polarization direction of the optical tweezers (x -axis). These two libration modes are described by the angles ϕ and θ , and both exhibit approximately the same characteristic frequency

$$\Omega_0 = \sqrt{\frac{\mathcal{E}^2(\alpha_3 - \alpha_1)}{2I_1}}, \quad (1)$$

where \mathcal{E} is the electric field amplitude in the center of the trap [16]. Since in thermal equilibrium we expect ϕ and θ to perform small-amplitude oscillations, i.e., $\sqrt{\frac{k_B T}{I_1 \Omega_0^2}} \ll 1$, we employ the small-angle approximation for ϕ and θ , which is equivalent to assuming a perfectly harmonic libration potential. The third rotational degree of freedom, ψ , is unconstrained if the particle is perfectly cylindrically symmetric. However, a slight asymmetry (specifically, a small difference between α_1 and α_2) can lead to a weak confinement of the intermediate axis along z , resulting in libration of ψ . This confinement can arise from both intensity gradient torques [8] and near-field effects due to strong focusing [28]. Experimental studies suggest that shape asymmetries are common in nominally spherical particles [8, 14].

The system is assumed to be in thermal equilibrium and all three rotational degrees of freedom of the nanodumbbell are subject to damping and are driven by the thermally fluctuating torques arising from the surrounding environment (gas in the vacuum chamber).

We model the dynamics of the Euler angles described above using the following equations of motion, which are derived from the Euler equations in the dumbbell's body frame [15, 16, 26]:

$$I_1 \ddot{\theta} + I_3 \dot{\phi} \dot{\psi} + I_1 \gamma_1 \dot{\theta} + I_1 \Omega_0^2 \theta = \tau_{\text{fl}, \theta}, \quad (2a)$$

$$I_1 \ddot{\phi} - I_3 \dot{\theta} \dot{\psi} + I_1 \gamma_1 \dot{\phi} + I_1 \Omega_0^2 \phi = \tau_{\text{fl}, \phi}, \quad (2b)$$

$$I_3 \ddot{\psi} + I_3 \gamma_3 \dot{\psi} + \frac{1}{2} I_3 \Omega_\psi^2 \sin 2\psi = \tau_{\text{fl}, \psi}, \quad (2c)$$

where thermal fluctuating torques are denoted as $\tau_{\text{fl}, \theta}$, $\tau_{\text{fl}, \phi}$ and $\tau_{\text{fl}, \psi}$; Ω_ψ is a parameter describing ψ confinement, and γ_1 and γ_3 are damping coefficients. The two harmonically oscillating libration modes, associated with angles ϕ and θ , are coupled, with a coupling strength proportional to $\dot{\psi}$. This type of coupling is characteristic of spinning top dynamics and causes the two degenerate libration modes to hybridize, splitting into distinct precession and nutation modes [16]. Consequently, the dynamics of the ψ angle become encoded in the motion of the long axis and, as will be shown later, determine the libration PSD of ϕ and θ .

The tight angular confinement of ϕ and θ justifies approximating their libration potentials as harmonic. However, this approximation does not hold for the weakly confined ψ angle, and therefore we retain its full sinusoidal potential in the form

$$U(\psi) = \frac{1}{4} I_3 \Omega_\psi^2 \cos(2\psi). \quad (3)$$

The corresponding deterministic torque term in Eq. (2c) is derived from this potential.

The fluctuating torques which are driving the particle follow the fluctuation-dissipation theorem,

$$\langle \tau_{\mathbb{H},i}(t_0) \tau_{\mathbb{H},j}(t_0 - t) \rangle = 2I_i \gamma_i k_B T \delta(t) \delta_{ij}, \quad (4)$$

and are modeled as

$$\tau_{\mathbb{H},\theta} = \sqrt{2I_1 \gamma_1 k_B T} \bar{\eta}_\theta(t), \quad (5a)$$

$$\tau_{\mathbb{H},\phi} = \sqrt{2I_1 \gamma_1 k_B T} \bar{\eta}_\phi(t), \quad (5b)$$

$$\tau_{\mathbb{H},\psi} = \sqrt{2I_3 \gamma_3 k_B T} \bar{\eta}_\psi(t), \quad (5c)$$

where $\eta_\theta(t)$, $\eta_\phi(t)$ and $\eta_\psi(t)$ are independent Wiener processes such that $\bar{\eta}_\theta(t)$, $\bar{\eta}_\phi(t)$ and $\bar{\eta}_\psi(t)$ represent their corresponding generalized derivatives.

III. ITO-TAYLOR EXPANSION BASED STOCHASTIC INTEGRATION SCHEME

In this section, we first recall the definition of Ito SDEs and outline the construction of stochastic integration schemes based on Ito's lemma and the Ito-Taylor expansion. We then present the associated multiple stochastic integrals and the generalized discretization scheme for multi-dimensional Wiener processes. Finally, we illustrate the solution of the underlying SDEs using the Ito-Taylor 1.5 scheme.

Consider the \mathcal{F}_t -measurable stochastic process, $y_k(t)$ under the filtered probability space $(S, \mathcal{F}, (\mathcal{F}_t)_{t \geq 0}, P)$ such that the governing Ito SDE for the d -dimensional diffusion process driven by m -dimensional Wiener process can be expressed as [19, 20],

$$dy_k(t) = a_k(t, y(t)) dt + \sum_{j=1}^m b_{k,j}(t, y(t)) dB^j(t),$$

with, $k = 1, 2, \dots, d$, (6)

where $a_k(t, y(t))$, $b_{k,j}(t, y(t))$ are the drift and diffusion coefficients, respectively, and $B^j(t)$ is the \mathcal{F}_t -measurable Wiener process with stationary independent increments following Gaussian distribution. The SDE in Eq. (6) has a unique solution if the drift and diffusion coefficients satisfy the Lipschitz and linear growth conditions [20]. For the solution of Eq. (6), numerical integration schemes of different orders of accuracy can be constructed by incorporating Ito's lemma in Eq. (6) in conjunction with integral form of Taylor series expansion [18, 20]. Considering all the first and second order multiple stochastic integrals (MSIs) along with one of the MSIs of multiplicity 3 from the Ito-Taylor expansion, the k^{th} component of Ito-Taylor 1.5 discretization for the solution to Eq. (6)

is written as [20],

$$\begin{aligned} y_k^{n+1} = & y_k^n + a_k \Delta t + \sum_{j=1}^m b_{k,j} \Delta B^j + \frac{1}{2} \mathfrak{S}^0 a_k (\Delta t)^2 \\ & + \sum_{j=1}^m (\mathfrak{S}^0 b_{k,j} I_{(0,j)} + \mathfrak{S}^j a_k I_{(j,0)}) \\ & + \sum_{j_1, j_2=1}^m \mathfrak{S}^{j_1} b_{k, j_2} I_{(j_1, j_2)} \\ & + \sum_{j_1, j_2, j_3=1}^m \mathfrak{S}^{j_1} \mathfrak{S}^{j_2} b_{k, j_3} I_{(j_1, j_2, j_3)}, \end{aligned} \quad (7)$$

where the expressions of the operators \mathfrak{S}^0 and \mathfrak{S}^j evaluated on the drift and diffusion coefficients are given as [20],

$$\begin{aligned} \mathfrak{S}^0(g(y(t))) = & \frac{\partial(g(y(t)))}{\partial t} + \sum_{k=1}^d a_k \frac{\partial(g(y(t)))}{\partial y_k} \\ & + \frac{1}{2} \sum_{k,l=1}^d \sum_{j=1}^m b^{k,j} b^{l,j} \frac{\partial^2(g(y(t)))}{\partial y_k \partial y_l}, \end{aligned} \quad (8a)$$

$$\mathfrak{S}^j(g(y(t))) = \sum_{k=1}^d b^{k,j} \frac{\partial(g(y(t)))}{\partial y_k}. \quad (8b)$$

The integral forms of the MSIs $I_{(0,j)}$, $I_{(j,0)}$, $I_{(j_1, j_2)}$ and $I_{(j_1, j_2, j_3)}$ in Eq. (7) can be phrased as [20],

$$I_{(0,j)} = \int_t^{t+\Delta t} \int_t^{s_1} ds_2 dB^j(s_1), \quad (9a)$$

$$I_{(j,0)} = \int_t^{t+\Delta t} \int_t^{s_1} dB^j(s_2) ds_1, \quad (9b)$$

$$I_{(j_1, j_2)} = \int_t^{t+\Delta t} \int_t^{s_1} dB^{j_1}(s_2) dB^{j_2}(s_1), \quad (9c)$$

$$I_{(j_1, j_2, j_3)} = \int_t^{t+\Delta t} \int_t^{s_1} \int_t^{s_2} dB^{j_3}(s_3) dB^{j_2}(s_2) dB^{j_1}(s_1), \quad (9d)$$

where Δt is the uniform step size of integration. For numerical implementation, the MSIs $I_{(j,0)}$ and $I_{(0,j)}$ in Eq. (9) can be expressed as [18, 20],

$$\begin{aligned} I_{(j,0)} = & \Delta Z^j, \\ I_{(0,j)} = & \Delta B^j \Delta t - I_{(j,0)}, \end{aligned} \quad (10)$$

with ΔB^j and ΔZ^j being the Brownian increments at each step [20]. Considering commutative noise of the second kind [20], the Ito-Taylor 1.5 discretization for multi-dimensional independent components of Wiener process

is obtained as,

$$\begin{aligned}
y_k^{n+1} = & y_k^n + a_k \Delta t + \sum_{j=1}^m b_{k,j} \Delta B^j + \frac{1}{2} \Im^0 a_k (\Delta t)^2 \\
& + \sum_{j=1}^m (\Im^0 b_{k,j} (\Delta B^j \Delta t - \Delta Z^j) + \Im^j a_k \Delta Z^j) \\
& + \frac{1}{2} \sum_{j=1}^m \Im^j b_{k,j} \left((\Delta B^{j_1})^2 - \Delta t \right) \\
& + \sum_{j_1=1}^m \sum_{j_2=1}^{j_1-1} \Im^{j_1} b_{k,j_2} \Delta B^{j_1} \Delta B^{j_2} \\
& + \frac{1}{2} \sum_{\substack{j_1, j_2=1 \\ j_1 \neq j_2}}^m \Im^{j_1} \Im^{j_2} b_{k,j_2} \Delta B^{j_1} \left((\Delta B^{j_2})^2 - \Delta t \right) \\
& + \sum_{j_1=1}^m \sum_{j_2=1}^{j_1-1} \sum_{j_3=1}^{j_2-1} \Im^{j_1} \Im^{j_2} b_{k,j_3} \Delta B^{j_1} \Delta B^{j_2} \Delta B^{j_3} \\
& + \frac{1}{2} \sum_{j=1}^m \Im^j \Im^j b_{k,j} \left(\frac{1}{3} (\Delta B^j)^2 - \Delta t \right) \Delta B^j. \quad (11)
\end{aligned}$$

For the most general case, i.e., for multiplicative noise, the numerical discretization in Eq. (11) has a strong order of accuracy of 1.5 [18]. For the equations of motion in Eqs.(2a)–(2c), consider the state-space representation as,

$$\begin{aligned}
y_1 := \theta, & \quad y_3 := \phi, & \quad y_5 := \psi, \\
y_2 := \dot{\theta}, & \quad y_4 := \dot{\phi}, & \quad y_6 := \dot{\psi}.
\end{aligned} \quad (12)$$

Accordingly, we express Eqs.(2a)–(2c) in the form of an Ito SDE (Eq. (6)) as follows,

$$\begin{aligned}
dy_1 &= y_2 dt, \\
dy_2 &= \left(-\frac{I_3}{I_1} y_4 y_6 - \gamma_1 y_2 - \Omega_0^2 y_1 \right) dt + \frac{c_1}{I_1} d\eta_\theta, \\
dy_3 &= y_4 dt, \\
dy_4 &= \left(\frac{I_3}{I_1} y_2 y_6 - \gamma_1 y_4 - \Omega_0^2 y_3 \right) dt + \frac{c_1}{I_1} d\eta_\phi, \\
dy_5 &= y_6 dt, \\
dy_6 &= \left(-\gamma_3 y_6 - \frac{1}{2} \Omega_\psi^2 \sin 2y_5 \right) dt + \frac{c_2}{I_3} d\eta_\psi, \quad (13)
\end{aligned}$$

where $c_1 = \sqrt{2I_1 \gamma_1 k_B T}$ and $c_2 = \sqrt{2I_3 \gamma_3 k_B T}$. The drift and diffusion coefficients can now be identified from Eq. (13) which are then used in Eq. (11) together with Eq. (8) to evaluate the trajectories of the state variables defined in Eq. (12). Based on Eqs. (12) and (5), k and m in Eq. (11) are 6 and 3 respectively.

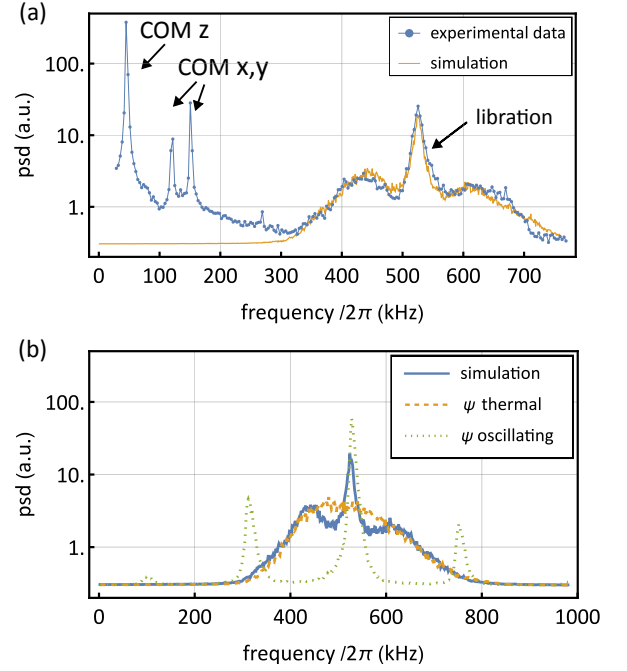


Figure 2. Power spectral densities. **(a)**: Experimental and simulated $S_{\phi\phi}(\omega)$. The libration motion appears as a peak with shoulders centered at 525 kHz. Cross-talk between detection channels results in COM oscillations visible in the experimental PSD at low frequencies. **(b)**: Simulated $S_{\phi\phi}(\omega)$ with a sinusoidal confinement potential for ψ , as per Eqs.(2a)–(2c). The dashed line shows the simulated $S_{\phi\phi}(\omega)$ in the absence of confinement for ψ ($\Omega_\psi = 0$), where the ψ motion is purely thermal. The dotted line corresponds to a scenario where the confinement potential for ψ is purely harmonic. The simulation time in all cases is 100 ms.

IV. RESULTS

A. Reference experimental data

We employed the stochastic simulation described previously to explain the rotational dynamics of the nanodumbbell studied experimentally in Ref. [15]. The nanodumbbell in question consists of two silica spheres, each with a nominal diameter of 143 nm. It is confined using linearly polarized optical tweezers operating at a wavelength of 1550 nm, with an optical power of 700 mW, and focused through a lens with a numerical aperture (NA) of 0.8. The particle is levitated at room temperature inside a vacuum chamber maintained at a pressure of 1.5 mbar. The angular trajectory $\phi(t)$ is inferred from polarization fluctuations in the trapping beam, introduced by light scattered from the particle (using forward-scattering scheme) [12]. The resulting libration power spectral density, shown in Fig. 2(a), is related to $\phi(t)$ as follows [29]:

$$S_{\phi\phi}(\omega) = \lim_{T \rightarrow \infty} \frac{\langle |\tilde{\phi}_T(\omega)|^2 \rangle}{T}, \quad (14)$$

where $\tilde{\phi}_T(\omega) = \frac{1}{2\pi} \int_{-T/2}^{T/2} dt \phi(t)e^{i\omega t}$ is a truncated Fourier transform and $\langle \cdot \rangle$ denotes the expectation value.

The libration mode ϕ is visible in Fig. 2(a) at 525 kHz, with lineshape characterized by a sharp central peak flanked by shoulders spaced approximately 100 kHz from the main peak. Although the measurement scheme is sensitive only to the ϕ angle [27], the libration detector also registers COM peaks due to cross-talk between the libration and COM detection channels. The COM motion along the beam propagation axis (z) is observed at 50 kHz, while the transverse COM modes (corresponding to particle oscillations along x and y) appear near 150 kHz.

B. Simulated libration power spectral density

The best-fit power spectral density $S_{\phi\phi}(\omega)$, obtained by simulating a 100 ms trajectory of all three angular degrees of freedom using our stochastic model and simulation framework, is shown alongside the experimental data in Fig. 2(a). The following parameters were fixed: the libration frequency $\Omega_0 = 2\pi \times 525$ kHz, the damping rates $\gamma_1 = \gamma_3 = 2\pi \times 1.5$ kHz, and the aspect ratio of the moments of inertia, $I_3/I_1 = 0.66$, consistent with a nanodumbbell characterized by a length-to-diameter ratio of 1.8. The free parameters in the simulation are the particle size characterized by the moment of inertia I_1 , with I_3 determined by a fixed aspect ratio and the confinement strength of the ψ degree of freedom, specified by the frequency Ω_ψ . To align the simulation with the experimental spectrum, the simulated power spectral density was additionally scaled by a calibration factor and offset by a constant baseline.

The simulation parameters yielding the best agreement with experimental data were $\Omega_\psi = 2\pi \times 220$ kHz and $I_1 = 2 \times 10^{-33}$ kg \cdot m². The value of Ω_ψ can be attributed to intensity gradient torques [8] and to the longitudinal field component arising from strong focusing [28]. However, the inferred moment of inertia I_1 is roughly an order of magnitude smaller than expected based on the nominal particle size and the density of silica. The value of I_1 determines the magnitude of thermal fluctuating torques in the simulation, according to Eq. (13). Possible explanations for this discrepancy include lower effective density of the particle and/or the presence of additional noise sources in the experiment, such as laser relative intensity noise (RIN), elevated local temperature, or coupling between the rotational and COM motion of the particle. The fact that the particle behaves as a much smaller one can be already deduced from the experimental data in Fig. 2(a): the observed sidebands appear approximately $\delta\Omega = 2\pi \times 180$ kHz apart. To explain the splitting of libration into two modes with frequencies $\delta\Omega$ apart, the particle would need to be spinning at $\dot{\psi} = \delta\Omega I_1/I_3 \approx 2\pi \times 273$ kHz [16]. In contrast, using the moment of inertia obtained from the nominal particle diameter and silica density, the expected spin-

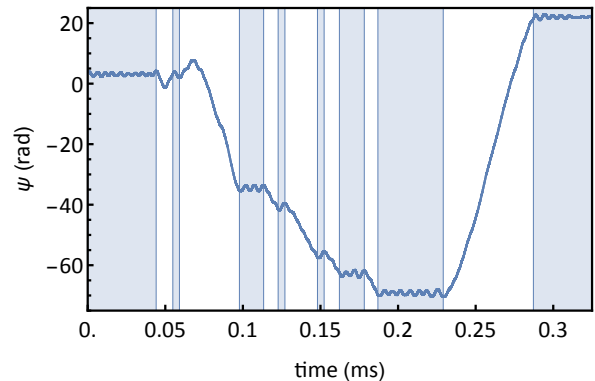


Figure 3. Fragment of a simulated trajectory $\psi(t)$. Shaded regions indicate periods of libration, where the intermediate axis oscillates around the z -direction. Unshaded regions correspond to the rotational regime, during which the particle spins around its long axis.

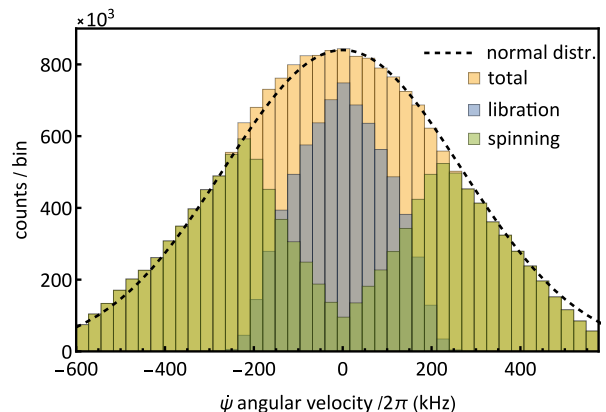


Figure 4. Histogram of the angular velocity distribution $\dot{\psi}$. The yellow region represents the total distribution over the full 100 ms simulation. The green region shows the distribution during rotational motion, while the blue region corresponds to periods of libration. The dashed line indicates a fitted normal distribution.

ning frequency (assuming the kinetic energy of $\frac{1}{2}k_B T$ associated with the long axis rotation) would be only $\dot{\psi} \approx 2\pi \times 87$ kHz.

C. Librating and rotating regime of the long axis rotation

For the simulation parameters that best reproduce the experimental power spectral density, the depth of the potential confining the angle ψ given by Eq. (3) (yielding $\frac{1}{4}I_3\Omega_\psi^2$), is on the order of $\frac{1}{2}k_B T$. Due to thermal fluctuations the particle alternates between two regimes: during certain intervals, the intermediate axis is trapped by the confining potential, resulting in oscillatory dynamics of ψ ; at other times, its energy exceeds the potential depth, allowing ψ to escape confinement and the particle to ro-

tate freely about its long axis. This behaviour is clearly visible in Fig. 3.

The effects of the two regimes of ψ motion are reflected in the shoulders flanking the libration peak. Figure 2(b) additionally shows what the power spectral density $S_{\phi\phi}(\omega)$ would look like in each regime: if the angle ψ rotated freely, the peak broadens into a rounded, Gaussian-like shape; if ψ were confined in a harmonic potential with natural frequency Ω_ψ , the peak becomes a Lorentzian with symmetric sidebands. These sidebands arise because the term $\dot{\theta}\dot{\psi}$ in Eq. (2b) has an effect similar to a torque oscillating at frequencies $\Omega_0 \pm \Omega_\psi$. Note that in the case of a sinusoidal (i.e., anharmonic) potential, the oscillations of the angle ψ span a range of frequencies extending up to a maximum of Ω_ψ , which results in broadened sidebands.

Fig. 4 further illustrates how the combination of rotational and librational regimes of the ψ angle gives rise to the shouldered peak structure observed in the libration PSD. When the particle rotates freely around its long axis, it cannot do so with low ψ values- if $\dot{\psi}$ becomes too small, the intermediate axis becomes confined by the potential, transitioning the particle back into the libration regime. As a result, thermal spinning (i.e., free rotation) occurs predominantly at high $\dot{\psi}$ velocities, leading to shouldered structure. Despite the transition between regimes, the total velocity distribution remains approximately Gaussian, following Maxwell-Boltzmann distribution. Analysis of the simulated 100 ms trajectory shows that in our case, the ψ degree of freedom spends approximately 53% of the time in the librating regime and 47% in the rotating regime.

To summarize, we identified that the phenomenon responsible for the observed libration peak with shoulders in optically trapped nanodumbbells is the long-axis rotation transitioning between librating and rotating regimes. Similar rotation-libration transitions have been studied for short-axis rotation [30, 31].

D. Effect of an additional torque spinning the particle along its long axis

To gain further insight into the effect of ψ confinement, we simulated the experimental conditions described in Fig. 3(a) of Ref. [15]. In that experiment, an additional beam applied a spinning (non-conservative) torque τ along the optical tweezers' polarization direction, causing the dumbbell to rotate around its long axis. The long-axis spinning speed increased until reaching a steady-state value of $\dot{\psi}_0 = \tau/(I_3\gamma_3)$. A simple theoretical model predicts that the originally degenerate libration modes hybridize into precession and nutation modes with frequencies given by

$$\Omega_{1/2} = \sqrt{\Omega_0^2 + g^2} \pm g, \quad (15)$$

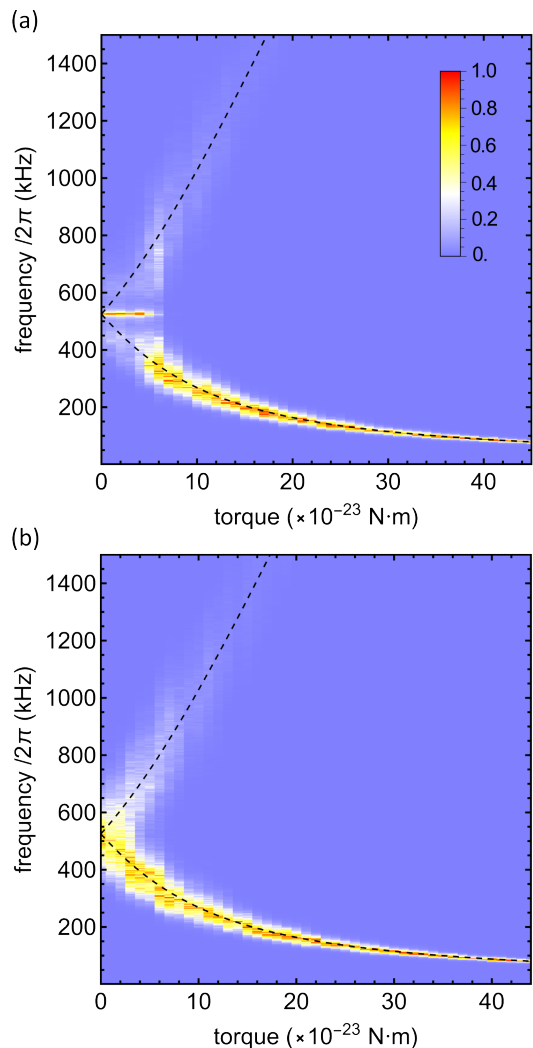


Figure 5. Libration PSD in arbitrary units, showing the effect of the spinning torque. Black dashed lines indicate the predicted precession and nutation frequencies calculated from Eq. (15). (a): Precession (low-frequency, narrow) and nutation (high-frequency, broad) modes emerge once the applied spinning torque exceeds a threshold value. (b): Same as (a), but without the confining potential ($\Omega_\psi = 0$).

where $g = (I_3/2I_1)\dot{\psi}_0$ [15]. However, this model did not predict the linewidths of these modes and failed to accurately describe the particle's behavior under small torque, where a threshold for mode splitting was observed. Notably, the libration mode retained its characteristic shoulder-like peak and only transitioned to distinct precession and nutation modes once the applied torque exceeded a certain minimum value.

Our stochastic modeling and simulation, in turn, shows that the intermediate axis sinusoidal potential described by Eq. (3) is responsible for the threshold. The spinning torque has been modelled by including an additional torque term τ in Eq. (2c), so that it becomes

$$I_3\ddot{\psi} + I_3\gamma_3\dot{\psi} + \frac{1}{2}I_3\Omega_\psi^2 \sin 2\psi = \tau + \tau_{fl,\psi}, \quad (16)$$

while Eqs. (2a) and (2b) remain unchanged.

The simulation results shown in Fig. 5(a) qualitatively reproduce both the threshold behavior and the experimentally observed linewidths of the precession and nutation modes. The threshold corresponds to the minimum non-conservative torque required to overcome the confining potential of the intermediate axis, enabling the dumbbell to spin persistently in the direction of the applied torque. For comparison, Fig. 5(b) presents simulation results without the ψ confinement potential, i.e., with $\Omega_\psi = 0$. In this case, no threshold is observed, and the precession and nutation frequencies are accurately described by Eq. (15).

V. CONCLUSION

This paper presented a stochastic simulation framework and a related model to reconstruct the complex dynamics of long-axis rotation (ψ)- a degree of freedom not directly accessible through experiments, by analyzing the readily detectable short-axis rotation (ϕ). The proposed simplification of the full nonlinear rotational dynamics was demonstrated to be sufficient for explaining and modelling benchmark experimental data Refs. [14, 15]. The proposed model and framework can be readily extended to include the remaining nonlinear terms from the complete equations of motion, as well as couplings to the COM degrees of freedom [32, 33]. Consequently, it has

the potential to be relevant in a generalised sense to understand the motion of high-aspect-ratio particles subject to strong coupling between rotational and translational motion, as well as for accurately reconstructing dynamics in engineered optical potential landscapes created by strongly focused structured light [7, 34].

The proposed Ito-Taylor expansion based stochastic integration approach can generate a complete trajectory of all three rotational degrees of freedom- including key nonlinearities within seconds on a standard laptop. This computational efficiency makes the method a practical and powerful tool for modeling and validation of rotational optomechanics experiments, along with development of new applications around high-precision devices measuring kinematic outputs.

VI. ACKNOWLEDGEMENTS

Joanna Zielinska acknowledges the support by Challenge-Based-Research project with the ID CLEIC_CLS_S_116 at Tecnológico de Monterrey. JZ also acknowledges the Photonics Laboratory at ETH Zurich, where she was previously based and where the experiments reported here were carried out. Ankush Gogoi and Vikram Pakrashi acknowledge the support of Research Ireland NexSys (21/SPP/3756) and Harmoni 22FFP-P11457.

-
- [1] Carlos Gonzalez-Ballester, Markus Aspelmeyer, Lukas Novotny, Romain Quidant, and Oriol Romero-Isart. Levitodynamics: Levitation and control of microscopic objects in vacuum. *Science*, 374(6564):eabg3027, 2021.
 - [2] David C Moore and Andrew A Geraci. Searching for new physics using optically levitated sensors. *Quantum Science and Technology*, 6(1):014008, 2021.
 - [3] M. Rossi, A. Militaru, N. Carlon Zambon, A. Riera-Campenya, O. Romero-Isart, M. Frimmer, and L. Novotny. Quantum delocalization of a levitated nanoparticle. *Phys. Rev. Lett.*, 135:083601, Jun 2025.
 - [4] Lorenzo Dania, Oscar Schmitt Kremer, Johannes Piotrowski, Davide Candoli, Jayadev Vijayan, Oriol Romero-Isart, Carlos Gonzalez-Ballester, Lukas Novotny, and Martin Frimmer. High-purity quantum optomechanics at room temperature. *Nature Physics*, pages 1–6, 2025.
 - [5] Tom Delord, P Huillery, L Nicolas, and G Hétet. Spin-cooling of the motion of a trapped diamond. *Nature*, 580(7801):56–59, 2020.
 - [6] Peng Ju, Yuanbin Jin, Kunhong Shen, Yao Duan, Zhu-jing Xu, Xingyu Gao, Xingjie Ni, and Tongcang Li. Near-field ghz rotation and sensing with an optically levitated nanodumbbell. *Nano letters*, 23(22):10157–10163, 2023.
 - [7] Yanhui Hu, Jack J Kingsley-Smith, Maryam Nikkhov, James A Sabin, Francisco J Rodríguez-Fortuño, Xiaohao Xu, and James Millen. Structured transverse orbital angular momentum probed by a levitated optomechanical sensor. *Nature Communications*, 14(1):2638, 2023.
 - [8] Mitsuyoshi Kamba, Ryoga Shimizu, and Kiyotaka Aikawa. Nanoscale feedback control of six degrees of freedom of a near-sphere. *Nature Communications*, 14(1):7943, 2023.
 - [9] A Pontin, H Fu, M Toroš, TS Monteiro, and PF Barker. Simultaneous cavity cooling of all six degrees of freedom of a levitated nanoparticle. *Nature Physics*, pages 1–6, 2023.
 - [10] Jialiang Gao, Fons van der Laan, Joanna A. Zielińska, Andrei Militaru, Lukas Novotny, and Martin Frimmer. Feedback cooling a levitated nanoparticle’s libration to below 100 phonons. *Phys. Rev. Res.*, 6:033009, Jul 2024.
 - [11] Jiangwei Yan, Xudong Yu, Zheng Vitto Han, Tongcang Li, and Jing Zhang. On-demand assembly of optically levitated nanoparticle arrays in vacuum. *Photonics Research*, 11(11):600, 4 2023.
 - [12] Fons van der Laan, Felix Tebbenjohanns, René Reimann, Jayadev Vijayan, Lukas Novotny, and Martin Frimmer. Sub-kelvin feedback cooling and heating dynamics of an optically levitated librator. *Phys. Rev. Lett.*, 127:123605, Sep 2021.
 - [13] Fons van der Laan, René Reimann, Andrei Militaru, Felix Tebbenjohanns, Dominik Windey, Martin Frimmer, and Lukas Novotny. Optically levitated rotor at its thermal limit of frequency stability. *Phys. Rev. A*, 102:013505,

- Jul 2020.
- [14] J. A. Zielińska, F. van der Laan, A. Norrman, M. Rimplinger, R. Reimann, L. Novotny, and M. Frimmer. Controlling optomechanical libration with the degree of polarization. *Phys. Rev. Lett.*, 130:203603, May 2023.
- [15] J. A. Zielińska, F. van der Laan, A. Norrman, R. Reimann, M. Frimmer, and L. Novotny. Long-axis spinning of an optically levitated particle: A levitated spinning top. *Phys. Rev. Lett.*, 132:253601, Jun 2024.
- [16] T Seberson and F Robicheaux. Parametric feedback cooling of rigid body nanodumbbells in levitated optomechanics. *Physical Review A*, 99(1):013821, 2019.
- [17] Jaehoon Bang, Troy Seberson, Peng Ju, Jonghoon Ahn, Zhujing Xu, Xingyu Gao, Francis Robicheaux, and Tongcang Li. Five-dimensional cooling and nonlinear dynamics of an optically levitated nanodumbbell. *Physical Review Research*, 2(4):043054, 2020.
- [18] Peter E Kloeden and Eckhard Platen. *Numerical Solution of Stochastic Differential Equations, First ed., Vol. 23. Stochastic Modelling and Applied Probability*. Berlin, Germany: Springer Science & Business Media, 1992.
- [19] Tapas Tripura, Ankush Gogoi, and Budhaditya Hazra. An Ito–Taylor weak 3.0 method for stochastic dynamics of nonlinear systems. *Appl. Math. Model.*, 86:115–141, 2020.
- [20] Ankush Gogoi, Satyam Panda, and Budhaditya Hazra. A computational framework for mean square responses of bidirectional nonlinear systems under correlated stochastic excitation. *J. Sound Vib.*, 523:116689, 2022.
- [21] Nayan Deep Tiwari, Ankush Gogoi, Budhaditya Hazra, and Qinhuo Wang. A shape memory alloy-tuned mass damper inerter system for passive control of linked-SDOF structural systems under seismic excitation. *J. Sound Vib.*, 494:115893, 2021.
- [22] Paul Mucchielli, Ankush Gogoi, Budhaditya Hazra, and Vikram Pakrashi. A mathematically consistent stochastic simulation of a 3d pendulum tuned mass damper and tuning. *Nonlinear Dyn.*, 109(2):401–418, 2022.
- [23] Kai Zeng, Xiangming Xu, Yulie Wu, Xuezhong Wu, and Dingbang Xiao. Optically levitated micro gyroscopes with an mhz rotational vaterite rotor. *Microsystems & Nanoengineering*, 10(1):78, 2024.
- [24] Benjamin A Stickler, Klaus Hornberger, and MS Kim. Quantum rotations of nanoparticles. *Nature Reviews Physics*, 3(8):589–597, 2021.
- [25] Eric W. Weisstein. Euler angles. *From MathWorld—A Wolfram Web Resource*.
- [26] L. D. Landau and E. M. Lifshitz. *Mechanics, Third Edition: Volume 1 (Course of Theoretical Physics)*. Butterworth-Heinemann, 3 edition, January 1976.
- [27] Felix Tebbenjohanns, Andrei Militaru, Andreas Norrman, Fons van der Laan, Lukas Novotny, and Martin Frimmer. Optimal orientation detection of an anisotropic dipolar scatterer. *Phys. Rev. A*, 105:053504, May 2022.
- [28] Lukas Novotny and Bert Hecht. *Principles of nano-optics*. Cambridge university press, 2012.
- [29] X Rong Li. *Probability, random signals, and statistics*. CRC press, 2017.
- [30] Stefan Kuhn, Alon Kosloff, Benjamin A Stickler, Fernando Patolsky, Klaus Hornberger, Markus Arndt, and James Millen. Full rotational control of levitated silicon nanorods. *Optica*, 4(3):356–360, 2017.
- [31] L. Bellando, M. Kleine, Y. Amarouchene, M. Perrin, and Y. Louyer. Giant diffusion of nanomechanical rotors in a tilted washboard potential. *Phys. Rev. Lett.*, 129:023602, Jul 2022.
- [32] M Rademacher, A Pontin, JMH Gosling, PF Barker, and M Toroš. Roto-translational optomechanics. *arXiv preprint arXiv:2507.20905*, 2025.
- [33] M. Kamba and K. Aikawa. Revealing the velocity uncertainties of a levitated particle in the quantum ground state. *Physical Review Letters*, 131:183602, Oct 2023.
- [34] Yahong Chen, Fei Wang, Zhen Dong, Yangjian Cai, Andreas Norrman, José J. Gil, Ari T. Friberg, and Tero Setälä. Structure of transverse spin in focused random light. *Phys. Rev. A*, 104:013516, Jul 2021.